Y-Modified MCM-22 Supported PdO$_x$ Nanocrystal Catalysts for Catalytic Oxidation of Toluene

Zhu Chen, Danna Situ, Jie Zheng, Zhen Cheng, Zhuo Wang and Shufeng Zuo *

Zhejiang Key Laboratory of Alternative Technologies for Fine Chemicals Process, Shaoxing University, Shaoxing 312000, China; chenzhu1127@163.com (Z.C.); stdn981@163.com (D.S.); zjie0807@sohu.com (J.Z.); chengzhen1993@126.com (Z.C.); zhuowang97@163.com (Z.W.)

* Correspondence: sfzuo@usx.edu.cn; Tel.: +86-575-8834-5681; Fax: +86-575-8834-5682

Abstract: A series of rare earth elements (REEs)-modified and Mobil Composition of Matter (MCM)-22-supported Pd nanocrystal catalysts were synthesized via a high-temperature solution-phase reduction method and tested for toluene complete oxidation. These catalytic materials were systematically characterized by N$_2$ adsorption/desorption, X-ray powder diffraction (XRD), scanning electron microscopy (SEM), high-resolution transmission electron microscopy (HRTEM), energy-dispersive spectroscopy (EDS), inductively coupled plasma atomic emission spectroscopy (ICP-AES), temperature-programmed surface reaction of toluene (toluene-TPSR) and X-ray photoelectron spectroscopic (XPS) techniques in order to investigate the structure–catalytic property relationship. Moreover, catalysts with an appropriate yttrium content greatly improved the catalytic activity of 0.2%Pd/MCM-22. PdO$_x$ (x = 0, 1) nanoparticles, ranging from 3.6 to 6.8 nm, which were well distributed on the surface of MCM-22. Efficient electron transfer from the Pd^{2+}/Pd^0 redox cycle facilitated the catalytic oxidation process, and the formation of Pd (or Y) –O–Si bonds improved the high dispersion of the PdO$_x$ and Y$_2$O$_3$ particles. Toluene–TPSR experiments suggested that the addition of Y$_2$O$_3$ improved the physical/chemical adsorption of 0.2%Pd/MCM-22, thus increasing the toluene adsorption capacity. Then, 0.2%Pd/7.5%Y/MCM-22 exhibited the highest catalytic performance. In addition, this catalyst maintained 95% conversion with high resistance to water and chlorine poisoning, even after toluene oxidation at 210 °C for 100 h, making it more valuable in practical applications.

Keywords: PdO$_x$ nanocrystal; MCM-22; Y$_2$O$_3$; toluene; catalytic oxidation

---

1. Introduction

Volatile organic compounds (VOCs) emitted from manufacturing, petrochemical refinement, and vehicle emissions are some of the prime air pollutants that cause persistent and cumulative influences on human health and the ecological environment [1–3]. Among various ways to eliminate VOCs, catalytic oxidation is considered to be one of the most efficient and environmentally friendly control technologies, since it can convert VOCs into CO$_2$ and H$_2$O at low temperatures [4,5].

To date, the catalysts employed for catalytic oxidation can be broadly classified into three categories: (i) noble metal-based catalysts (Pd, Pt, Ru, Au, Ag, etc.), (ii) transition metal oxide-based catalysts, and (iii) rare earth metal oxide-based catalysts [6–9]. Supported noble metal catalysts are often used in toluene and various VOC catalytic oxidation processes due to their preferable catalytic activity and stability, despite their high cost [10,11]. In terms of Pd-based catalysts, their economic efficiency and excellent performance on the oxidation of hydrocarbons has received considerable attention [12,13]. The choice of support has an important influence on the VOC catalytic oxidation activity of Pd-based catalysts. Supports used include molecular sieves, pillared clay, TiO$_2$, γ-Al$_2$O$_3$,

CeO_2, etc. [14–20]. Mobil Composition of Matter (MCM)-22 zeolite with MWW topology which was named by international zeolite association was adopted as a support, and the confinement of the pores can effectively prevent the agglomeration of Pd particles, thereby achieving the effective utilization of noble metal catalysts. This material consists of two independent 10-membered ring (MR) pore systems. The first pore system is composed of two-dimensional (2D) sinusoidal channels (4.0 Å × 5.0 Å) with circular 10-MR and the second one is composed of three-dimensional (3D) 12-MR supercages with inner diameters of 7.1 Å and heights of 18.2 Å interconnected by 10-MR channels (4.0 Å × 5.5 Å) [21–23]. Due to the unique porous structure, MCM-22 has potential applications in hydrocarbon catalytic oxidation. To the best of our knowledge, rare earth elements (REEs) play the role of a promoter that can improve thermal stability, resistance to poisoning, and catalytic activity. Fan et al. [24] investigated how the presence of Ce improved the dispersion of PdO particles and maintained the amount of Pd^{2+} and retarded sintering during the methane combustion process, thus increasing the catalytic activity and thermal stability of Pd-Pt/Al_2O_3. Kotolevich et al. [25] reported that Ce and La oxides-modified TiO_2-supported Au significantly influenced their catalytic properties in n-octanol oxidation. In a study by Yue et al. [26], the introduction of Y to Pd/Ce-Zr/Al_2O_3 improved catalytic activity and thermal stability, possibly by inhibiting the decomposition of PdO particles and improving the reduction–reoxidation performance of active PdO. He et al. [27] reported that the incorporation of Y promoted the diffusion of lattice oxygen and enhanced lattice oxygen mobility on the catalyst. Consequently, it is reasonable to assume that the combination of REE-modified MCM-22 supports palladium in order to improve its catalytic performance.

The present work is dedicated to developing an efficient and stable catalyst for toluene complete oxidation. A series of REEs/MCM-22-supported Pd catalysts were designed and prepared by a simple high-temperature solution-phase reduction method, and the catalysts with 7.5%Y were determined to have the best catalytic activity. Based on characterization results and catalytic properties, the promotion role of yttrium is discussed. The catalysts prepared by the traditional impregnation method have the disadvantages of large particle size and uneven dispersion, but the method adopted in this paper can solve the above problems, thus remarkably improving the catalytic activity. In this paper, the influence of Y loading on the structure of MCM-22 and properties of the Pd catalysts has been systematically explored to develop an efficient nanocatalyst for complete toluene oxidation.

2. Results and Discussion

2.1. Catalytic Activity and Durability Test

As shown in Figure 1a, the catalytic activity of Pd/MCM-22 with different REEs (Y, Ce, La, Pr, and Nd) was evaluated for toluene oxidation. As seen, the catalytic activity was greatly improved after catalysts were modified with REEs. The order of promotion effect was as follows: Y > Pr > Nd > Ce > La, indicating that the best REEs was Y. It showed that 0.2%Pd/5%Y/MCM-22 achieved a complete conversion of toluene at 240 °C compared to 0.2%Pd/MCM-22 at 340 °C. As presented in Figure S1, the catalytic activity of 0.2%Pd/MCM-22 synthesized by a traditional impregnation method was also tested. Regarding the two different methods, 0.2%Pd/MCM-22 prepared by the high-temperature solution-phase reduction method had higher catalytic activity for toluene oxidation.

The effect of Y content is also investigated in Figure 1b. Notably, the catalyst with 7.5 %Y possessed the highest catalytic activity, and the toluene conversion reached 100% at about 220 °C. The conversion greatly increased from 14% to 95% as the Y loading increased from 0 up to 7.5 wt. %, demonstrating that Y_2O_3 acted as a promoter. However, a further increase in the content of Y_2O_3 on Pd/MCM-22 resulted in a significant decrease in catalytic activity, probably because some PdO_x active sites were covered by excessive Y_2O_3.
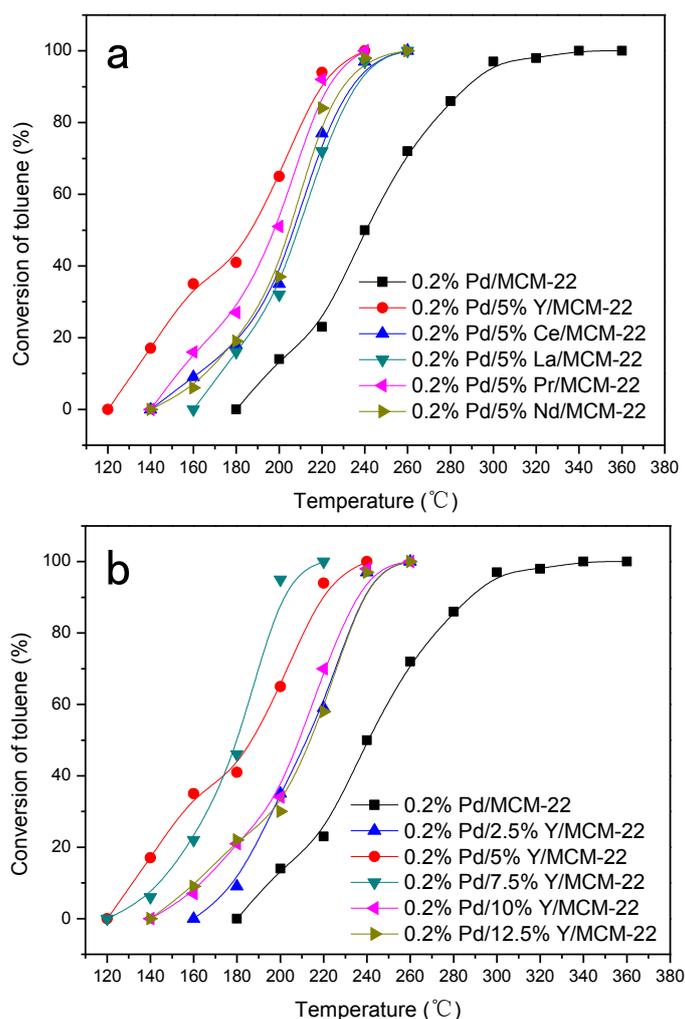
Figure 1. (**a**) Influence of the addition of rare earth into Pd/MCM-22 for toluene complete oxidation; (**b**) influence of the content of Y into Pd/MCM-22 for toluene complete oxidation. Toluene concentration: 1000 ppm; gas hourly space velocity (GHSV): 20,000 h^{-1}.

The durability test of 0.2%Pd/7.5%Y/MCM-22 at 210 °C for 100 h is shown in Figure 2. The conversion of toluene was constant and remained at approximately 95%, which indicated that this catalyst had superior catalytic stability for toluene oxidation. In practical application, water vapor and chlorobenzene widely exist in waste gases. As shown in Figure 2, in the first step, after introducing 100 ppm chlorobenzene into the reaction system, the toluene conversion continuously dropped from 95% to 90%. This can be reasonably attributed to the competitive adsorption/oxidation on the active sites. In the second step, a 3% water steam was introduced into the process. The downward trend was more obvious and toluene conversion further decreased from 90% to 84%, which was caused by the competitive adsorption effect of water. Interestingly, the toluene conversion almost returned to the initial level of 94% after removal of water and chlorobenzene, indicating that 0.2%Pd/7.5%Y/MCM-22 had excellent resistance to water and chlorobenzene. For a heterogeneous-catalyzed reaction, the catalyst durability plays a significant role in the practical application.
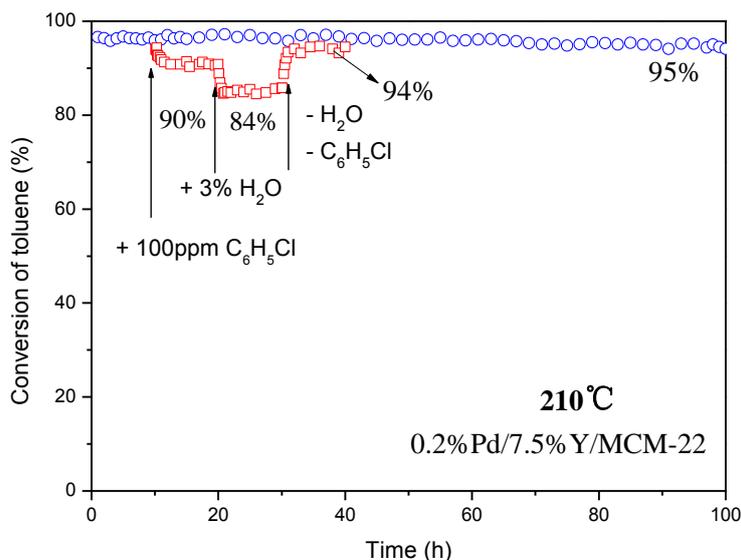
Figure 2. Durability test for toluene oxidation over the 0.2%Pd/7.5%Y/MCM-22 catalyst (reacted at 210 °C). The blue symbol: under a dry air condition; the red symbol: in the presence of water and chlorobenzene.

2.2. Characterization Section

2.2.1. XRD

The XRD patterns of samples are shown in Figure 3. For MCM-22, it exhibited three different distinctive characteristics {(100), (220), (310)}. Furthermore, the absence of an interlayer diffraction line at 6.5° (200) indicated condensation of the layers during calcination, resulting in an ordered three-dimensional structure. Obviously, the characteristic peaks of MCM-22 were found in the XRD patterns of all the catalysts. Moreover, the characteristic diffraction peaks of PdO were not observed, indicating that PdO was highly dispersed on the surface of MCM-22 and/or the catalysts had a low Pd content. In addition, no diffraction peaks attributed to Y_2O_3 were detected in the XRD patterns of 0.2%Pd/7.5%Y/MCM-22, confirming that Y_2O_3 was highly dispersed or Y_2O_3 existed in the amorphous state because a low calcination temperature (400 °C) was detrimental to the formation of metal oxide crystalline [28]. In addition, the diffraction peaks of MCM-22 became broader with a weaker intensity, which may reflect the lattice distortion and the crystalline grain size reduction due to Y_2O_3 doping.

2.2.2. N_2 Adsorption/Desorption

Nitrogen adsorption/desorption isotherms and pore distributions were used to investigate the textural properties of all the samples. The relevant curves and data are shown in Figure 4 and Table 1. Generally, this instrument is mainly used for mesoporous analysis. The presence of microporous parts cannot be observed in Figure 4a,b, but the microporous data in Table 1 is accurate. As shown in Figure 4a, all isotherms were similar and can be identified as type IV with a H3-type hysteresis loop according to International Union of Pure and Applied Chemistry (IUPAC), which occurred at a relative pressure range of 0.5–1.0, indicating the presence of mesoporous structures in all samples. Figure 4b shows the corresponding pore size distribution. MCM-22 and 0.2%Pd/MCM-22 exhibited pore size distributions centered at 4.0 and 25.6 nm; the pore size distribution was kept almost constant after Pd loading, which was indicative of the unblocked mesopores. However, after the addition of yttrium, the larger pore size was reduced to 18.2 nm. It can be concluded that the large Y_2O_3 particles were formed and the main part of Y_2O_3 was distributed in the larger pore size of the MCM-22. From Table 1, MCM-22 has both the highest S_{BET} of 466.5 m^2/g and V_p of 0.55 cm^3/g. The S_{BET}, V_p, and V_{mic} tended to decrease after loading the active component PdO_x and Y_2O_3 promoter, which was probably due to the partial pore blocking of the channels by aggregated metal particles. Overall, 0.2%Pd/7.5%Y/MCM-22 still exhibited

the high S_{BET} and V_p, which were beneficial for the catalytic oxidation of toluene by providing a good diffusion condition to increase the amount of reactive edge sites [29].
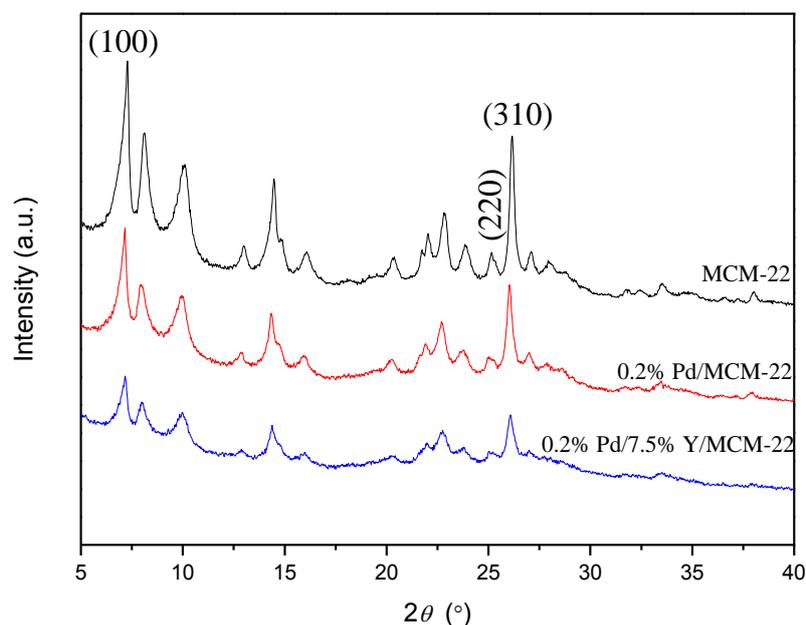
Figure 3. XRD patterns of the samples.

Table 1. Textural properties of all samples. MCM: Mobil Composition of Matter.

Samples	S_{BET}^{a} (m²/g)	A_{mes} $(A_{mic})^{b}$ (m²/g)	V_P^{c} (cm³/g)	V_{mic}^{d} (cm³/g)
MCM-22	466.4	161.1 (305.3)	0.55	0.14
0.2%Pd/MCM-22	391.6	144.4 (247.2)	0.55	0.11
0.2%Pd/7.5%Y/MCM-22	264.1	89.4 (174.7)	0.34	0.081

[a] S_{BET} = total specific surface area. [b] A_{mes} = the area of mesopore, evaluated from the t-plot method; the area of micropore (A_{mic}) is obtained by subtracting A_{mes} from the total surface area (S_{BET}). [c] V_p = total pore volume, from the amount adsorbed at the relative pressure of 0.969. [d] V_{mic} = micropore volume, calculated by the t-plot method.

2.2.3. SEM and HRTEM

Detailed morphological information for catalysts are obtained by SEM characterization (Figure 5). As presented in Figure 5a,b, the SEM images of MCM-22 showed the platelet-like morphology of the well-known MWW zeolite, which was arranged in larger spherical secondary particles. These platelets appeared to be more than 1 μm in size. The lamellar crystals of MCM-22 have an average length of about 100–250 nm and an average thickness of about 25 nm. From Figure 5c, the microstructure possessed the flake morphology, but no Pd nanoparticles were visible. However, after adding Y_2O_3 (Figure 5d), the morphology changed and became rougher and thicker, probably because a large amount of Y_2O_3 covered the surface, and the uniform distribution of Y_2O_3 was observed by the EDS of Figure S2, which was well consistent with the XRD results.

HRTEM characterization of all samples is shown in Figure 6. Figure 6a,b was consistent with SEM micrographs in term of size and morphology. As presented in Figure 6c,d, it can be observed that many black spots (PdO_x) were dispersed throughout MCM-22, and it was remarkable that 0.2%Pd/7.5%Y/MCM-22 (presented in Figure 6d) showed a higher dispersity of PdOx nanoparticles compared to 0.2%Pd/MCM-22 (presented in Figure 6c). As can be seen from Figure S3, the PdO_x nanoparticles had a size distribution of 3.7–10.9 nm, and the average size was 7.3 nm over 0.2%Pd/MCM-22. After the introduction of Y_2O_3, the average size of the PdO_x nanoparticles decreased to 5.2 nm. This finding suggested that the existence of Y_2O_3 improved the dispersion of PdO_x

nanoparticles. Furthermore, the EDS and corresponding elemental mapping are presented in Figure S4, which confirms that Pd and Y elements have been successfully loaded in MCM-22 support.
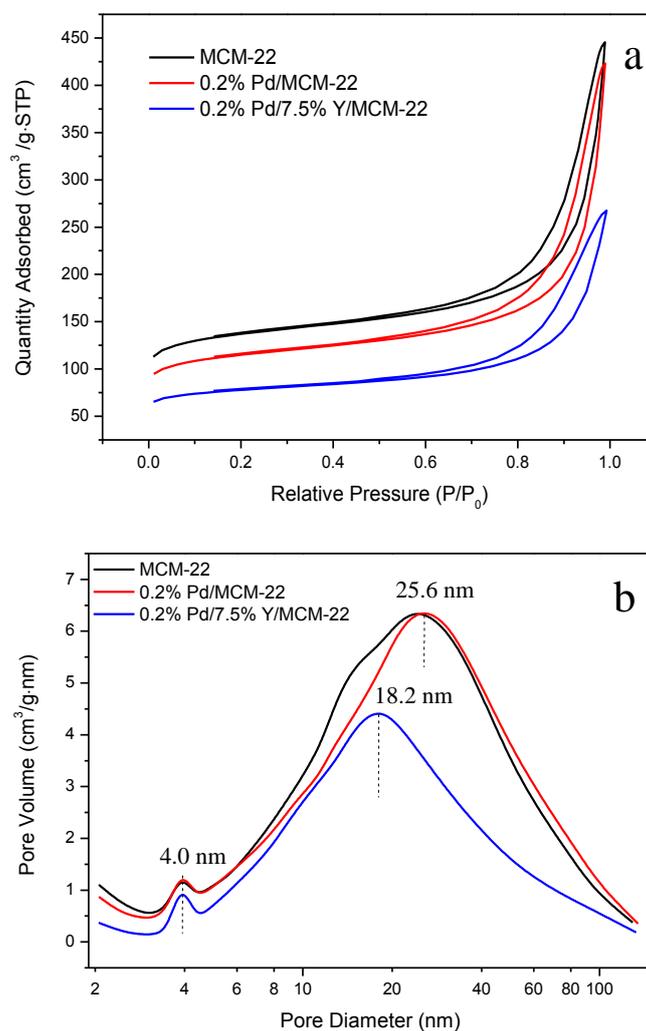
Figure 4. Textural properties of the samples: (**a**) adsorption/desorption isotherms; (**b**) pore size distributions.

2.2.4. ICP and CO Chemisorption

The actual Pd loading and Pd dispersion of catalysts are summarized in Table 2. 0.2%Pd/MCM-22 and 0.2%Pd/7.5%Y/MCM-22 were measured by ICP analysis to identify palladium content. The results indicated that the theoretical and actual quantities of Pd nanoparticles matched well, which were similar to our desired 0.2 wt. % Pd loading. Pd dispersion was further determined by CO chemisorption. Among the catalysts, Pd dispersion on 0.2%Pd/7.5%Y/MCM-22 was calculated to be 43%, which was much higher than that on 0.2%Pd/MCM-22 (22%), because Y_2O_3 can greatly promote the dispersion of PdO_x nanoparticles. As we know, high dispersion of the active particles is a major factor in promoting catalytic activity, because more active centers are exposed to the surface of the support.
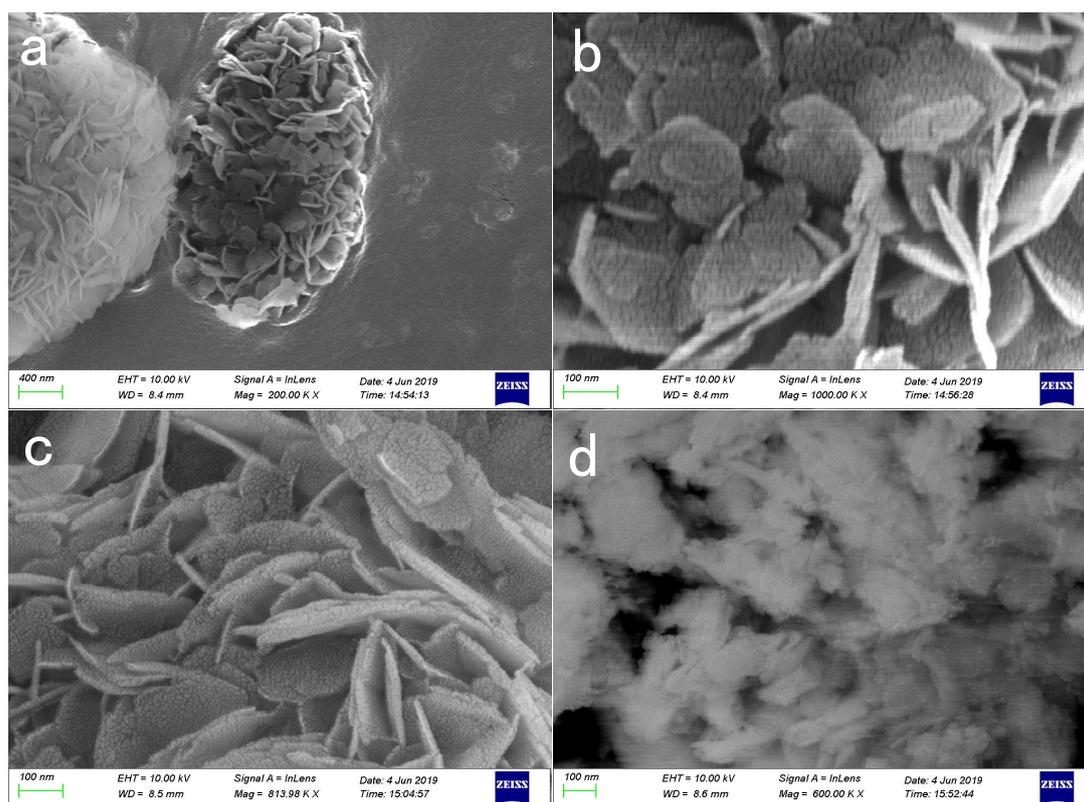
Figure 5. SEM images of (**a,b**) MCM-22; (**c**) 0.2%Pd/MCM-22; (**d**) 0.2%Pd/7.5%Y/MCM-22.
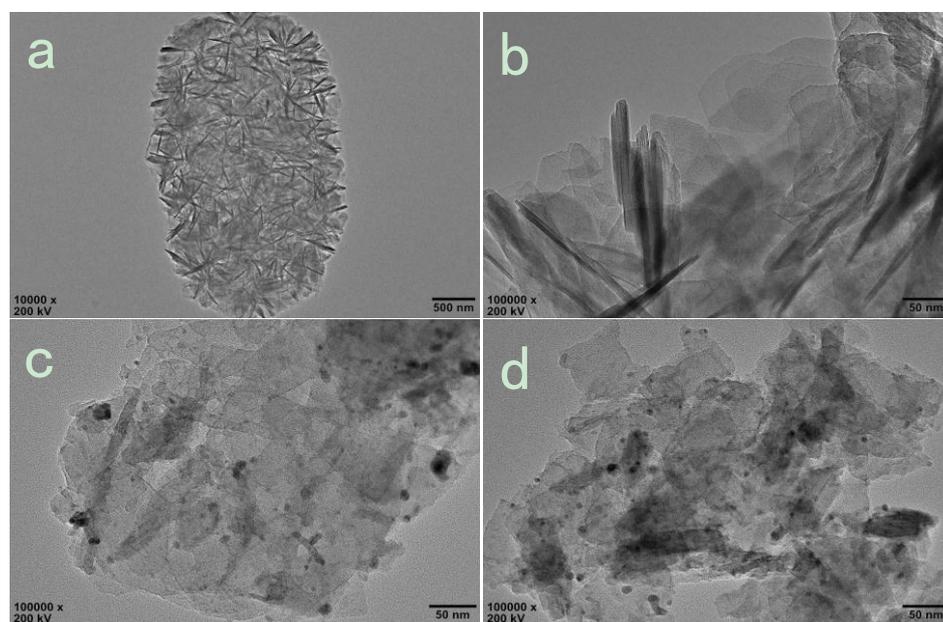
Figure 6. HRTEM images of (**a,b**) MCM-22; (**c**) 0.2%Pd/MCM-22; (**d**) 0.2%Pd/7.5%Y/MCM-22.

Table 2. Summary of the characterization results for all catalysts.

Catalysts	Pd Species	3d$_{5/2}$ BE/ev	3d$_{3/2}$ BE/eV	Conc. [a] (%)		Pd Content [b] (wt. %)	Pd Dispersion [c] (%)
				Pd^{2+}	Pd^0		
0.2%Pd/MCM-22	**Pd^0**	**335.3**	**339.8**	**71.1**	28.9	0.19	22
	Pd^{2+}	336.6	342.1				
0.2%Pd/7.5%Y/MCM-22	Pd^0	335.3	340.5	73.3	26.7	0.18	43
	Pd^{2+}	336.3	341.8				
0.2%Pd/7.5%Y/MCM-22-used	Pd^0	335.3	340.5	47.8	52.2	0.18	41
	Pd^{2+}	336.5	342.1				

[a] Determined by X-ray photoelectron spectroscopic (XPS). [b] Determined by inductively coupled plasma atomic emission spectroscopy (ICP-AES). [c] Determined by CO chemisorption.

2.2.5. XPS

The Pd three-dimensional (3D) spectra of 0.2%Pd/MCM-22 (fresh) and 0.2%Pd/7.5%Y/MCM-22 (fresh and used) are shown in Figure 7a. Based on the binding energy reported in the literature and the symmetric peaks, it can be clearly seen that two states of palladium are presented on the surface of these catalysts [30]. The two characteristic peaks of Pd 3d$_{3/2}$ and Pd 3d$_{5/2}$ for the Pd^0 metallic state are at 339.8–340.5 eV and 335.3 eV, respectively. The characteristic peaks of Pd 3d$_{3/2}$ and Pd 3d$_{5/2}$ at 341.8–342.1 eV and 336.3–336.5 eV are assigned to the Pd^{2+} cationic state. Figure 7b shows that the Y 3d$_{3/2}$ and Y 3d$_{5/2}$ peaks are centered at about 158.0 eV and 160.0 eV, respectively. The energy difference between them was 2.0 eV, which proved that the valence state of Y was +3. Apparently, there was no significant difference between the Y 3d signals of 0.2%Pd/7.5%Y/MCM-22 (fresh and used), meaning that Y$_2$O$_3$ cannot be reduced during the catalytic oxidation of toluene. As shown in Figure S5, the O1s peak of 0.2%Pd/MCM-22 was formed by the superposition of O1s peaks of SiO$_2$ (532.7 eV), PdO (530.1 eV). Meanwhile, a large amount of SiO$_2$ existed in the catalyst, so the peak of O 1s appeared at 532.5 eV. After the addition of Y$_2$O$_3$, the intensity of the O 1s peak was weakened, since the formation of Pd (or Y) –O–Si bonds improved the high dispersion of the metal particles on the surface [28].

For fresh 0.2%Pd/7.5%Y/MCM-22, the binding energies of Pd 3d XPS peaks shifted to a lower value due to the transfer of electron to Pd. In addition, slight shifts of 1.1 eV and 1.2 eV to higher binding energy were observed compared to the standard binding energy of Y 3d$_{3/2}$ (158.9 eV) and Y 3d$_{5/2}$ (156.8 eV), indicating that the electron has been transferred from Y. Overall, this phenomenon indicated that electrons have been transferred from Y to Pd, suggesting that an interaction existed between the promoter and metal [31].

As shown in Table 2, the ratio of Pd^{2+} showed an increase from 71.1% (0.2%Pd/MCM-22-fresh) to 73.3% (0.2%Pd/7.5%Y/MCM-22-fresh). It can be found that the introduction of Y$_2$O$_3$ changed the surface atomic ratios of Pd^{2+} and Pd^0 of the catalysts, so that the catalyst had greater amounts of Pd^{2+}, which provided active sites. XPS analysis of the Pd species on 0.2%Pd/7.5%Y/MCM-22 (fresh and used) was carried out to identify its transformation after use. The used catalyst exhibited the highest amount of Pd^0, indicating that the divalent state became zero valence after the catalytic oxidation of toluene. The co-existence of Pd^0 and Pd^{2+} led to the high activity for the toluene, and the conversion rate between Pd^{2+} and Pd^0 is proportional to the entire catalytic oxidation process (Pd↔PdO) [32]. Therefore, the valence transformation of Pd was a key factor in improving the catalytic performance.
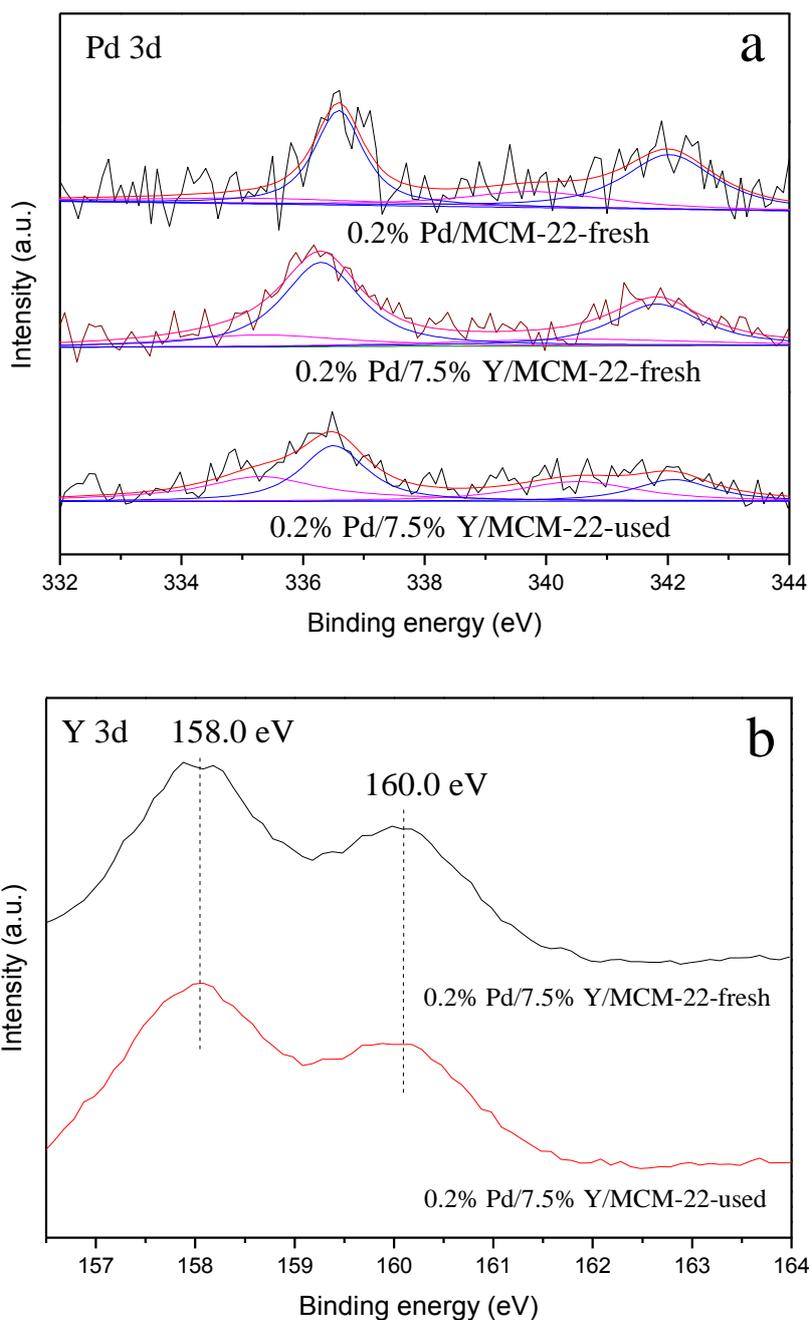
Figure 7. XPS spectra of the catalysts: (**a**) Pd (3d); (**b**) Y (3d).

2.2.6. Toluene-TPSR

The temperature-programmed surface reaction of toluene (toluene-TPSR) profiles for 0.2%Pd/MCM-22 and 0.2%Pd/7.5%Y/MCM-22 are shown in Figure 8. It is well known that the adsorption–desorption properties of the reactants have a great influence on the catalytic activity of the catalysts. As shown in Figure 8a, the penetration times of the two catalysts were different: 16.2 min for 0.2%Pd/MCM-22, and 19.4 min for 0.2%Pd/7.5%Y/MCM-22. Here, 0.2% Pd/7.5%Y/MCM-22 had a larger adsorption capacity, while the V_p was smaller than that of 0.2%Pd/MCM-22. We deduced that Y_2O_3 greatly enhanced the physical/chemical adsorption of toluene to Pd/MCM-22, thereby increasing the adsorption capacity and adsorption strength.
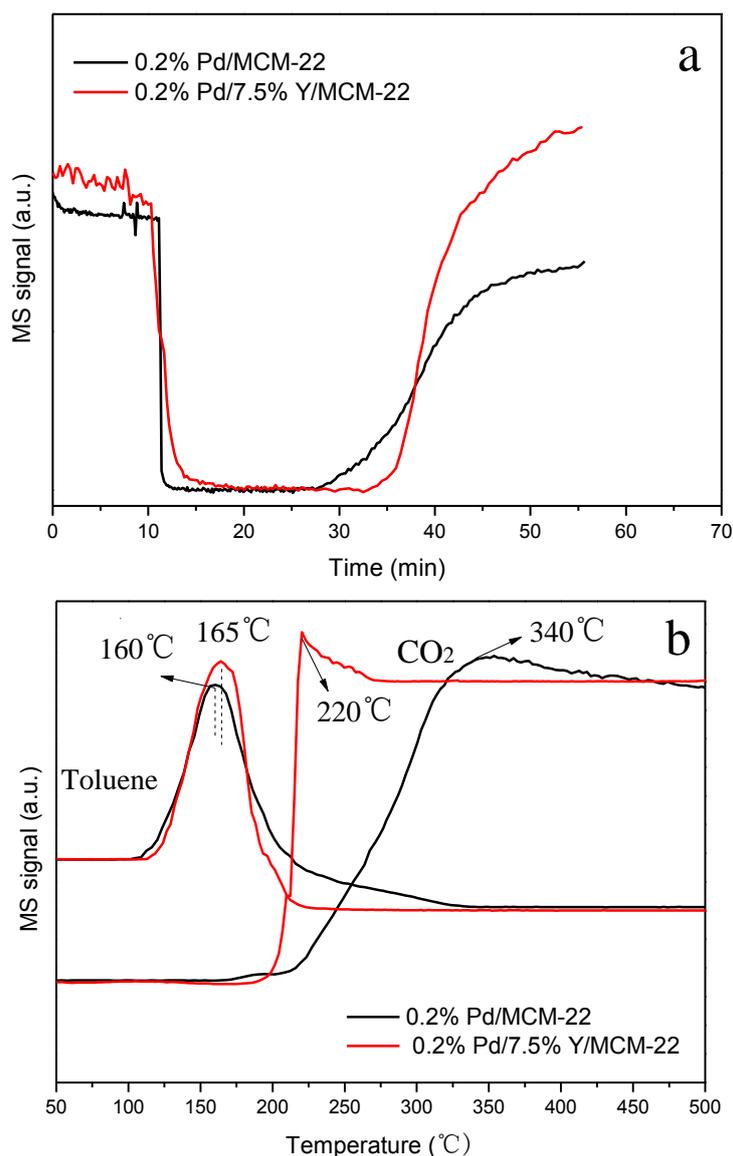
Figure 8. Toluene-TPSR profiles for (**a**) adsorption and (**b**) desorption.

As presented in Figure 8b, the toluene desorption peak of 0.2%Pd/7.5%Y/MCM-22 appeared at a higher temperature (165 °C) than that of 0.2%Pd/MCM-22 (160 °C). Meanwhile, the intensity of the peak of toluene desorption for 0.2%Pd/7.5%Y/MCM-22 was slightly stronger, which indicated that the catalyst had a higher adsorption ability for toluene. As the temperature further increased, the MS signals of CO_2 and toluene reached a stable stage, which meant that toluene had been completely oxidized to CO_2 and H_2O. Notably, only the final products (CO_2 and H_2O) were detected during the entire progress, suggesting that both catalysts exhibited excellent deep oxidation activity. Moreover, the concentration–temperature curve of CO_2 was consistent with the trend of toluene degradation conversion.

3. Experimental Section

3.1. Catalysts Preparation

MCM-22 was prepared by hydrothermal synthesis based on procedures described elsewhere [33]. The composition of the reaction mixture was $SiO_2/Al_2O_3 = 30$, $Na/SiO_2 = 0.29$, hexamethyleneimine (HMI)/$SiO_2 = 0.6$, HMI/Na = 2.08, and $H_2O/SiO_2 = 30$.

5%REEs/MCM-22 (REEs = Y, Ce, La, Pr, and Nd) were prepared by the impregnation method in our previous research [9]. x%Y/MCM-22 (x = 2.5, 5, 7.5, 10, 12.5) were prepared with different contents of Y. The % symbol in catalysts represents the mass percentage.

First, 0.2%Pd/REE/MCM-22 and 0.2%Pd/x%Y/MCM-22 were synthesized via the high-temperature solution-phase reduction method. Typically, 2.0 g of MCM-22 powders dissolved in 100 mL of ethylene glycol was added to a three-neck flask before stirring at 30 °C for 30 min. Then, 0.4 mL of H_2PdCl_4 (10 mg/mL), the Pd precursor, was added dropwise to the homogeneous mixture. Then, the mixture was stirred at 2000 r/min with N_2 flow passing through the reaction system for 12 h. The NaOH was subsequently added to the mixture until the pH reached approximately 11. The mixture was heated at 165 °C for 3 h. After cooling to 30 °C, the solid was collected by centrifugation and washed three times with deionized water and once with ethanol to ensure that no chloride or ethylene glycol remained. After drying at 60 °C overnight in an air atmosphere, the solid was finally calcined at 400 °C for 2 h in a muffle furnace.

3.2. Catalytic Activity Determination

The activity of the catalysts for toluene oxidation was evaluated with a continuous flow microreactor (WFS-3010, Xianquan, Tianjin, China). The reactive flow (1000 ppm toluene in air) was fed at 125 mL/min with a gas hourly space velocity (GHSV) of approximately 20,000 h^{-1}. In a typical measurement, catalyst (0.375 mL, 40–60 mesh) was loaded in the central part of the quartz tube. The concentration of toluene was monitored by on-line gas chromatography (GC-14C, Shimadzu, Kyoto, Japan) equipped with a flame ionization detector (FID) using an SE-30 capillary column both before and after the simulated gases passed through the microreactor. The durability test was carried out under the same condition at 210 °C.

3.3. Temperature-Programmed Reactions

The temperature-programmed surface reaction of toluene (toluene-TPSR) was carried out using 200 mg of catalyst. Before the experiment, the catalyst was pretreated in air at 300 °C for 0.5 h, and then cooled down to 50 °C. The O_2/Ar flow was switched to a mixture containing 100 mL/min O_2/Ar + 1000 ppm toluene until the complete adsorption of toluene. Finally, a toluene-TPSR run was started at a heating rate of 7.5 °C/min to 500 °C. GC-MS (QGA, Hiden, Warrington, UK) was used for the on-line monitoring of effluent gases.

3.4. Catalysts Characterization

The crystalline structures of the catalysts were obtained by powder XRD (PANalytical, Almelo, Netherlands) with nickel-filtered Cu Kα radiation. The X-ray tube was operated at 40 kV between 5° and 40°, with a step size of 0.02 and a speed of 4°/min.

Nitrogen adsorption–desorption isotherms of the samples were carried out at –195.8 °C on a TristarII 3020 apparatus instrument (Micromeritics Company, Atlanta, GA, USA) for surface textural analysis, including specific surface area (S_{BET}), mesopore area (A_{mes}), micropore area (A_{mic}), total pore volume (V_p), and micropore volume (V_{mic}). All of the samples were degassed at 200 °C for 4 h before testing. The pore size distributions were determined by the Barrett–Joyner–Halenda (BJH) desorption dV/dlog(D) method.

Scanning electron microscopy (SEM) of samples were performed using a ZEISS Sigma 300 instrument equipped with an Oxford X-Max energy-dispersive spectroscopy (EDS) detector. All samples were coated with a conducting gold film and held on a carbon tape.

High-resolution transmission electron microscopy (HRTEM) scans were obtained on a JEM-2010 electron microscope at an accelerating voltage of 200 kV. The sample powders were prepared by dispersing in ethanol using ultrasound for 10 min. A few droplets of the suspension were dropped onto carbon-coated copper grids. The elemental distribution was measured using energy-dispersive spectroscopy (EDS, Oxford Instruments, Warrington, UK). The histograms of the size distribution were

composed by measuring the size of more than 100 particles in several areas of the grid. The mean size of Pd particles (D_{Pd}) was calculated by the equation $D_{Pd} \approx \sum n_i D_i / \sum n_i$, where n_i is the particles number, and D_i is the particle diameter.

The content of Pd in the catalysts was analyzed using inductively coupled plasma atomic emission spectroscopy (ICP-AES) on a Leeman ICP-AES Prodigy XP (Leeman Labs, Hudson, NH, USA). Typically, the catalysts were dissolved in aqua regia and diluted with deionized water prior to determination.

CO chemisorption tests were performed on a CHEMBET-3000 apparatus (Quantachrome Instruments, Boynton Beach, FL, USA) to estimate the dispersion of particles by the pulse method. The catalyst was first reduced in H_2 at 400 °C for 1 h, and then the temperature decreased to room temperature in flowing He. Finally, several pulses of CO were injected into the sample until the sample reached complete saturation. Pd dispersion was calculated from the amount of CO chemisorption by assuming a stoichiometric ratio atomic of CO:Pd = 1:1.

X-ray photoelectron spectroscopic (XPS) characterization was conducted on a Thermo Scientific Escalab250Xi X-ray Photoelectron Spectrometer (Thermo Fisher Scientific, Waltham, MA, USA) using Al Kα (hν = 1486.6 eV). The C1s peak located at 284.6 eV was used as the internal standard reference to calibrate electron binding energies.

4. Conclusions

In this work, a series of rare earth elements (REEs) modified and MCM-22-supported PdO_x nanocrystal catalysts were prepared by a high-temperature solution-phase reduction method and used for a catalytic complete oxidation of toluene. The catalyst test showed that the catalytic activity of REEs-modified Pd/MCM-22 catalysts was higher than that of 0.2%Pd/MCM-22 for toluene oxidation, and 0.2%Pd/7.5%Y/MCM-22 exhibited the highest catalytic performance. XPS analysis showed that metal, promoter, and support interaction contributed to the dispersion of PdO_x and Y_2O_3 particles, and the introduction of Y_2O_3 improved the amounts of Pd^{2+}, which provided active sites. Toluene-TPSR experiments suggested that the addition of Y_2O_3 improved the physical/chemical adsorption of Pd/MCM-22, which was helpful to the oxidation reaction. The characterizations of the textural properties, metal composition, elemental distribution, and morphology verified the excellent catalytic performance of 0.2%Pd/7.5%Y/MCM-22. The catalyst exhibited complete toluene oxidation at 220 °C and proved to be perfectly stable at 210 °C for 100 h.

Supplementary Materials: The following are available online at http://www.mdpi.com/2073-4344/9/11/902/s1, Figure S1. The comparison of different preparation methods on the catalytic activity of 0.2%Pd/MCM-22, Figure S2. SEM-EDS elemental (Y) mapping image of 0.2%Pd/7.5%Y/MCM-22, Figure S3. Histograms with the paticle size distribution of 0.2%Pd/MCM-22 and 0.2%Pd/7.5%Y/MCM-22, Figure S4. HRTEM-EDS elemental mapping images of 0.2%Pd/MCM-22 and 0.2%Pd/7.5%Y/MCM-22, Figure S5. XPS spectra of O 1s over fresh 0.2%Pd/MCM-22 and 0.2%Pd/7.5%Y/MCM-22.

Author Contributions: Z.C. (Zhu Chen) did most of the characterization and was responsible for writing. D.S., J.Z. and Z.W. performed the catalytic studies and catalyst characterization. Z.C. (Zhen Cheng) conducted the XPS analysis. S.Z. designed the experiments, helped in the writing, and supervised the work. All authors contributed to the data interpretation and discussion.

Funding: This research was supported by the National Natural Science Foundation of China (21577094), Zhejiang Province Public Welfare Technology Research Project (LGG19B070003) and the Foundation of Science and Technology of the Shaoxing City (2018C10019).

Conflicts of Interest: The authors declare no conflict of interest.

References

1.　Hu, J.; Li, W.B.; Liu, R.F. Highly efficient copper-doped manganese oxide nanorod catalysts derived from CuMnO hierarchical nanowire for catalytic combustion of VOCs. *Catal. Today* **2018**, *314*, 147–153. [CrossRef]

2.　Chen, J.; Chen, X.; Chen, X.; Xu, W.J.; Xu, Z.; Jia, H.P.; Chen, J. Homogeneous introduction of CeO_y into MnO_x-based catalyst for oxidation of aromatic VOCs. *Appl. Catal. B Environ.* **2018**, *224*, 825–835. [CrossRef]

3. Kamal, M.S.; Razzak, S.A.; Hossain, M.M. Catalytic oxidation of volatile organic compounds (VOCs)–A review. *Atmos. Environ.* **2016**, *140*, 117–134. [CrossRef]

4. Zhu, A.M.; Zhou, Y.; Wang, Y.; Zhu, Q.L.; Liu, H.Y.; Zhang, Z.K.; Lu, H.F. Catalytic combustion of VOCs on Pt/CuMnCe and Pt/CeY honeycomb monolithic catalysts. *J. Rare Earths* **2018**, *36*, 1272–1277. [CrossRef]

5. Tang, W.X.; Wu, X.F.; Liu, G.; Li, S.D.; Li, D.Y.; Li, W.H.; Chen, Y.F. Preparation of hierarchical layer-stacking Mn-Ce composite oxide for catalytic total oxidation of VOCs. *J. Rare Earths* **2015**, *33*, 62–69. [CrossRef]

6. Gluhoi, A.C.; Nieuwenhuys, B.E. Catalytic oxidation of saturated hydrocarbons on multicomponent Au/Al$_2$O$_3$ catalysts: Effect of various promoters. *Catal. Today* **2007**, *119*, 305–310. [CrossRef]

7. Kim, S.C. The catalytic oxidation of aromatic hydrocarbons over supported metal oxide. *J. Hazard. Mater.* **2002**, *91*, 285–299. [CrossRef]

8. Lin, H.Q.; Chen, Y.W. Complete oxidation of toluene on Pd/modified-CeO$_2$ catalysts. *J. Taiwan Inst. Chem. Eng.* **2016**, *67*, 69–73. [CrossRef]

9. Yang, P.; Li, J.R.; Chen, Z.; Zuo, S.F. Promoting effects of Ce and Pt addition on the destructive performances of V$_2$O$_5$/γ-Al$_2$O$_3$ for catalytic combustion of benzene. *Appl. Catal. A Gen.* **2017**, *542*, 38–46. [CrossRef]

10. Santos, V.P.; Carabineiro, S.A.C.; Tavares, P.B.; Pereira, M.F.R.; Órfão, J.J.M.; Figueiredo, J.L. Oxidation of CO, ethanol and toluene over TiO$_2$ supported noble metal catalysts. *Appl. Catal. B Environ.* **2010**, *99*, 198–205. [CrossRef]

11. Matějová, L.; Topka, P.; Jirátová, K.; Šolcová, O. Total oxidation of model volatile organic compounds over some commercial catalysts. *Appl. Catal. A Gen.* **2012**, *443*, 40–49. [CrossRef]

12. Khder, A.E.R.S.; Altass, H.M.; Orif, M.I.; Ashour, S.S.; Almazroai, L.S. Preparation and characterization of highly active Pd nanoparticles supported Mn$_3$O$_4$ catalyst for low-temperature CO oxidation. *Mater. Res. Bull.* **2019**, *113*, 215–222. [CrossRef]

13. Xiong, H.F.; Wiebenga, M.H.; Carrillo, C.; Gaudet, J.R.; Pham, H.N.; Kunwar, D.; Oh, S.H.; Qi, G.; Kim, C.H.; Datye, A.K. Design considerations for low-temperature hydrocarbon oxidation reactions on Pd based catalysts. *Appl. Catal. B Environ.* **2018**, *236*, 436–444. [CrossRef]

14. Ye, N.; Li, Y.; Yang, Z.; Zheng, J.; Zuo, S.F. Rare earth modified kaolin-based Cr$_2$O$_3$ catalysts for catalytic combustion of chlorobenzene. *Appl. Catal. A Gen.* **2019**, *579*, 44–51. [CrossRef]

15. Abbasi, Z.; Haghighi, M.; Fatehifar, E.; Saedy, S. Synthesis and physicochemical characterizations of nanostructured Pt/Al$_2$O$_3$-CeO$_2$ catalysts for total oxidation of VOCs. *J. Hazard. Mater.* **2011**, *186*, 1445–1454. [CrossRef] [PubMed]

16. Guo, Y.L.; Gao, Y.J.; Li, X.; Zhuang, G.L.; Wang, K.C.; Zheng, Y.; Sun, D.H.; Huang, J.L.; Li, Q.B. Catalytic benzene oxidation by biogenic Pd nanoparticles over 3D-ordered mesoporous CeO$_2$. *Chem. Eng. J.* **2019**, *362*, 41–52. [CrossRef]

17. Fu, X.R.; Liu, Y.; Yao, W.Y.; Wu, Z.B. One-step synthesis of bimetallic Pt-Pd/MCM-41 mesoporous materials with superior catalytic performance for toluene oxidation. *Catal. Commun.* **2016**, *83*, 22–26. [CrossRef]

18. Feio, L.S.; Escritori, J.C.; Noronha, F.B.; Hori, C.E. Combustion of butyl carbitol using supported palladium catalysts. *Catal. Lett.* **2008**, *120*, 229–235. [CrossRef]

19. Garcia, T.; Solsona, B.; Murphy, D.M.; Antcliff, K.L.; Taylor, S.H. Deep oxidation of light alkanes over titania-supported palladium/vanadium catalysts. *J. Catal.* **2005**, *229*, 1–11. [CrossRef]

20. Mitsui, T.; Matsui, T.; Kikuchi, R.; Eguchi, K. Low-temperature complete oxidation of ethyl acetate over CeO$_2$-supported precious metal catalysts. *Top. Catal.* **2009**, *52*, 464–469. [CrossRef]

21. Lim, T.H.; Nam, K.; Song, I.K.; Lee, K.Y.; Kim, D.H. Effect of Si/Al$_2$ ratios in Mo/H-MCM-22 on methane dehydroaromatization. *Appl. Catal. A Gen.* **2018**, *552*, 11–20. [CrossRef]

22. Martins, A.; Silva, J.M.; Henriques, C.; Ribeiro, F.R.; Ribeiro, M.F. Influence of rare earth elements La, Nd and Yb on the acidity of H-MCM-22 and H-Beta zeolites. *Catal. Today* **2005**, *107*, 663–670. [CrossRef]

23. Wang, Y.A.; Gao, Y.; Xie, S.J.; Liu, S.L.; Chen, F.C.; Xin, W.J.; Zhu, X.X.; Li, X.J.; Jiang, N.; Xu, L.Y. Adjustment of the Al siting in MCM-22 zeolite and its effect on alkylation performance of ethylene with benzene. *Catal. Today* **2018**, *316*, 71–77. [CrossRef]

24. Fan, X.; Wang, F.; Zhu, T.L.; He, H. Effects of Ce on catalytic combustion of methane over Pd-Pt/Al$_2$O$_3$ catalyst. *J. Environ. Sci.* **2012**, *24*, 507–511. [CrossRef]

25. Kotolevich, Y.; Kolobova, E.; Khramov, E.; Farías, M.H.; Zubavichus, Y.; Tiznado, H.; Martínez-González, S.; Corberán, V.C.; Mota-Morales, J.D.; Pestryakov, A.; et al. n-Octanol oxidation on Au/TiO$_2$ catalysts promoted with La and Ce oxides. *Mol. Catal.* **2017**, *427*, 1–10. [CrossRef]

26. Yue, B.H.; Zhou, R.X.; Zheng, X.M.; Lu, W.C. Remarkable improvement of yttrium on the activity and thermal stability of methane combustion over Pd/Ce-Zr/Al$_2$O$_3$ catalyst. *Mater. Chem. Phys.* **2009**, *114*, 722–727. [CrossRef]

27. He, H.; Dai, H.X.; Ng, L.H.; Wong, K.W.; Au, C.T. Pd-, Pt-, and Rh-loaded Ce$_{0.6}$Zr$_{0.35}$Y$_{0.05}$O$_2$ three-way catalysts: An investigation on performance and redox properties. *J. Catal.* **2002**, *206*, 1–13. [CrossRef]

28. Li, J.F.; Xia, C.; Au, C.T.; Liu, B.S. Y$_2$O$_3$-promoted NiO/SBA-15 catalysts highly active for CO2/CH$_4$ reforming. *Int. J. Hydrogen Energy* **2014**, *39*, 10927–10940. [CrossRef]

29. Li, L.Y.; Han, W.L.; Dong, F.; Zong, L.Y.; Tang, Z.C.; Zhang, J.Y. Controlled pore size of ordered mesoporous Al$_2$O$_3$-supported Mn/Cu catalysts for CO oxidation. *Micropor. Mesopor. Mater.* **2017**, *249*, 1–9. [CrossRef]

30. Zhang, Y.Y.; Zeng, H.; Jia, B.; Wang, Z.H.; Liu, Z.M. Selective catalytic reduction of NO$_x$ by H$_2$ over Pd/TiO$_2$ catalyst. *Chin. J. Catal.* **2019**, *40*, 849–855. [CrossRef]

31. Oemar, U.; Hidajat, K.; Kawi, S. High catalytic stability of Pd-Ni/Y$_2$O$_3$ formed by interfacial Cl for oxy-CO$_2$ reforming of CH$_4$. *Catal. Today* **2017**, *281*, 276–294. [CrossRef]

32. Baldwin, T.R.; Burch, R. Catalytic combustion of methane over supported palladium catalysts: II. Support and possible morphological effects. *Appl. Catal.* **1990**, *66*, 359–381. [CrossRef]

33. Marques, A.L.S.; Monteiro, J.L.F.; Pastore, H.O. Static crystallization of zeolites MCM-22 and MCM-49. *Micropor. Mesopor. Mater.* **1999**, *32*, 131–145. [CrossRef]